Biochemical Pharmacology 82 (2011) 1832–1842

Contents lists available at SciVerse ScienceDirect

Biochemical Pharmacology

journal homepage: www.elsevier.com/locate/biochempharm

Effects of the novel vascular targeting agent MDS-11P on tumor vascularity and its antitumor activity

Zhi-Ting Deng [a,1], Teng Feng [a,1], Peng Wang [a], Xin Qi [a], Xue-Hong Chen [a], Ying-Xia Li [a], Chun-Li Song [a], Mei-Yu Geng [b,**], Jing Li [a,*]

[a] Key Laboratory of Marine Drugs, Ministry of Education, School of Medicine and Pharmacy, Ocean University of China, 5 Yu-Shan Road, Qingdao 266003, China
[b] Division of Antitumor Pharmacology, State Key Laboratory of Drug Research, Shanghai Institute of Materia Medica (SIMM), Chinese Academy of Sciences, Shanghai 201203, China

ARTICLE INFO

Article history:
Received 9 July 2011
Accepted 31 August 2011
Available online 6 September 2011

Keywords:
Vascular disrupting agents
MDS-11P
Antitumor
CA4 derivative
Vascularity

ABSTRACT

Vascular disrupting agents show selective effects on tumor established vasculature, and achieve encouraging results in both pre-clinical and clinical experiments. In the present study, we investigated the effects of a new CA4 derivative MDS-11 and its prodrug MDS-11P on vascular disrupting activity *in vitro* and *in vivo*. Surface plasmon resonance (SPR) and tubulin polymerization assay showed that MDS-11 interacted with tubulin directly and inhibited tubulin polymerization in a cell free system, and western blot assay further confirmed the action in the cellular level. MDS-11 was found to significantly disrupt the microtubulin skeleton in proliferating HUVECs than quiescent ones determined by confocal microscopy. Furthermore, MDS-11 was found to damage the HUVEC-formed tube quickly, but did not influence structures of microvessels from aortic ring possessing pericytes and smooth muscle cells until 3 h treatment. In A549 xenograft mice, immunohistochemistry staining of tumor sections revealed that a single dose of MDS-11P led to large areas of necrosis within tumor and reduced the number of tumor vessels, which was consolidated by perfused vascular volume assay. Pharmacokinetic studies of MDS-11P indicated that MDS-11P rapidly converted to the active form, MDS-11, and exhibited a much faster elimination in mice. The antitumor analysis using H22 and A549 mice xenograft models revealed that the growth inhibition rates of MDS-11P at 50 mg/kg (twice a day for three weeks) reached 59.4%, 60.5% respectively without obvious weight loss. Taken together, these results suggest that MDS-11 is a potential vascular disrupting agent for further development of antitumor drug.

1. Introduction

It is now well established that most tumors would be unable to grow beyond a microscopic size of 1–2 mm^3 without recruiting new blood vessels. In 1971 Folkman first published a hypothesis that "tumor growth is angiogenesis dependent". Thereafter, therapeutic vascular targeting of tumors has concentrated on anti-angiogenic approaches, which aims to prevent the neovascularization processes in tumors. In recent years, the abnormal characteristics of tumor blood vessels in structure and function have been studied in the attempt to attack and destroy solid tumors. These vascular abnormalities consist of temporary occlusions, a rapidly dividing endothelial population, blind ends, leaky vessels, and a reduction in pericytes [1–3]. Tumor-vascular disrupting agents (VDAs) are a new class of anti-cancer drugs that show strong promise in treating a variety of solid tumors [4]. In contrast to antiangiogenic therapy, which inhibits the outgrowth of new blood vessels, VDAs treatments selectively attack the existing tumor vasculature. Several low-molecular-weight VDAs are currently in clinical trials or undergoing preclinical testing. The lead drug of this kind of agents is combretastatin A4 (CA4), which has been extensively examined in various preclinical and clinical trials and has achieved encouraging results.

CA4, originally isolated from the South African shrub, *Combretum caffrum*, has a high affinity for tubulin at the colchicine-binding site, causing destabilization of the cytoskeleton and inducing vascular collapse [5]. Converting the initial compound to combretastatin A4 disodium phosphate (combretastatin A4 prodrug, CA4P) improves its solubility in aqueous solution [6]. Under physiological conditions, the phosphate group is cleaved by endogenous nonspecific phosphatases, thereby transforming the prodrug into its biologically active form [7]. After treatment with

Abbreviations: AUC, areas under concentration-time curve; DMSO, dimethyl sulfoxide; MVD, microvessel density; PCNA, proliferating cell nuclear antigen; VDA, vascular-disrupting agent.

* Corresponding author. Tel.: +86 053282031980.
** Corresponding author.
E-mail addresses: mygeng@mail.shcnc.ac.cn (M.-Y. Geng), ljlilac@163.com (J. Li).

[1] These authors contributed equally to this work.

0006-2952/$ – see front matter © 2011 Elsevier Inc. All rights reserved.
doi:10.1016/j.bcp.2011.08.024

CA4P, endothelial cells have been observed to undergo shape changes as a consequence of cytoskeletal disrupting, which supposes to lead to the increase in vascular permeability. Finally, endothelial cells detach, the vascular wall collapses, and tumor cell death occurs as a consequence of tumor blood flow obstructions. CA4 has tumor vascular damaging effects at well-tolerated doses of CA4P in animal models [5,8,9]. CA4P has received orphan drug designation for the treatment of anaplastic thyroid cancer, medullary thyroid cancer, and stage IV papillary or follicular thyroid cancer. In spite of that, the most common toxicity of CA4P was tumor pain, which was not dose-limiting. Dose-limiting toxicities include chest pain and/or cardiotoxicity, reversible ataxia, vasovagal syncope and motor neuropathy. Therefore, there are numerous synthetic analogues by structural modification of the CA4P in order to develop new agents with more activity and fewer adverse reactions.

It has been reported that the double bond in CA4 is prone to be isomerized to the more thermally stable trans-isomer, resulting in the complete loss of cytotoxicity [10]. Wang et al. [11] demonstrated that the cis double bond in CA4 can be replaced by a 1, 2-disubstituted five membered heterocycle such as imidazole, oxazole, or pyrazole. Based on evidences, in our previous studies, more than thirty of CA4 analogues with oxazole instead of cis double bond were synthesized and screened for their binding affinity to tubulin and the activity to disrupt the morphology of nonconfluent HUVEC cells after 0.5 h treatment. Among them, compound MDS-11 exhibited moderate binding affinity and a prominent cellular activity. In the present study, anti-tumor effects of the MDS-11 and its prodrug MDS-11P at molecular, cellular and animal levels were respectively investigated.

2. Materials and methods

2.1. Preparation of compounds

For the *in vitro* studies, MDS-11 was dissolved in DMSO at a concentration of 10 mM and then subsequently diluted in culture medium. However, the limited solubility of MDS-11 created several technical difficulties, which were overcome by the synthesis of a more soluble derivative, MDS-11-phosphate (MDS-11P, prodrug), which makes an ideal prodrug because the phosphate group can be cleaved by endogenous nonspecific phosphatases (Fig. 1). MDS-11P was dissolved in PBS at 10 mM and subsequently diluted in a similar manner to that for the parent compound. For the *in vivo* experiments, MDS-11P was dissolved in 0.9% saline and injected i.p. at 0.01 ml/g body weight. Tumor-bearing mice were treated with either MDS-11P or CA4P at 100 mg/kg. CA4P acted as a positive control.

2.2. Cell culture

HUVECs were isolated as primary explants, according to the method of Baudin et al. [12]. Cells from umbilical vein were cultured on tissue culture grade plastic ware coated with 0.2% gelatin. They were maintained in medium M199 (Sigma, St. Louis, MO.), supplemented with 0.01% glutamine, 20% FCS, 20 μg/ml endothelial cell growth supplement (B&D, Bioscience, San Jose, CA) and 15 units/ml heparin (Sigma, St. Louis, MO). HUVECs of fourth to seventh passage were grown to confluence, then were trypsinized, suspended, and seeded into culture dishes or wells for experimental use.

Human lung adenocarcinoma cell line A549 was purchased from the Institute of Biochemistry and Cell Biology (Shanghai, China), and maintained according to the suppliers' instructions.

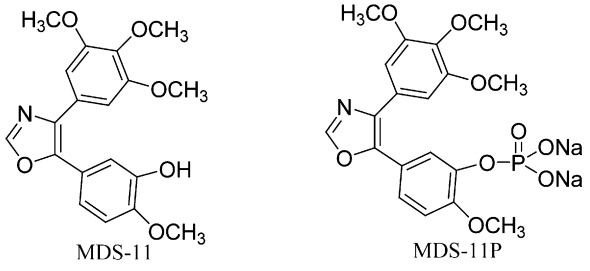

Fig. 1. Structural diagram of MDS-11 and its prodrug MDS-11P.

2.3. Animals and tumors

Male Balb/cA nu/nu and KM mice, ages 6–8 weeks and average body weight of 18 g, were obtained from Shanghai Laboratory Animal Center, Chinese Academy of Sciences (Shanghai, China). Mice were given access to food and water *ad libitum*. The use of animals was approved by Institutional Animal Care and Use Committee, with confirm adherence to the ethical guide lines for the care and use of animals. H22-bearing mice and male Sprague Dawley rats were purchased from Shanghai Laboratory Animal Center, Chinese Academy of Sciences (Shanghai, China).

2.4. Surface plasmon resonance analysis

The kinetics and specificity of the binding reactions between MDS-11 and tubulin were carried out with the BIAcore surface plasmon resonance apparatus (BIAcore X, Uppsala, Sweden). Briefly, tubulin was immobilized on CM5 sensor chips according to the reference reported [13]. To assess real-time binding capacity, 35 μl soluble MDS-11 or CA4 or colchicine was injected over the sensor chip surface with the immobilized tubulin, followed by washing with HBS-EP buffer for 5 min. The sensor chip surface was regenerated using 60 μl NaCl (2 M). All binding experiments were performed at 25 °C with a constant flow rate of 10 ml/min HBS-EP. For binding affinity assessment, the association phase was allowed to proceed to equilibrium. To correct for nonspecific binding and bulk refractive index change, a blank channel without MDS-11 was employed as a control for each experiment. Sensor grams for all binding interactions were recorded in real time and analyzed after subtracting that from the blank channel. Changes in mass due to the binding response were recorded as resonance units (Ru). Binding kinetics and affinities were determined by SPR using BIACORE software 3.1.

2.5. Tubulin turbidity assays

Tubulin was prepared from porcine brains using the assembly–disassembly method [14]. The tested drugs at various concentrations were first mixed with purified tubulin in a 96-well plate on ice. After placing the plate into a 37 °C incubator, tubulin polymerization was initiated and monitored by turbidity changes at 340 nm using a spectrometer (SpectraMAX190, Molecular Devices, Sunnyvale, CA). The reaction buffer for the assay contained 80 mM PIPES (pH 6.9), 0.5 mM EGTA, 2 mM $MgCl_2$ and 1 mM GTP.

2.6. Microtubule destabilization assay in cells

HUVECs were grown in 6-well plates, and then exposed to MDS-11 at concentrations of 0.1 μM, 1 μM for 30 min. Cells harvested in hypotonic lysis buffer [1 mM EGTA, 1 mM $MgCl_2$, 30% glycerol, 5% DMSO, 5 mM GTP, 1% NP-40, 0.1 mM PIPES (pH 6.9), and protease inhibitors]. Samples were centrifuged at 180,000 × *g* for 1 h at 37 °C in a temperature-controlled Eppendorf centrifuge model

5402 to separate the pellet (polymerized fraction) from the supernatant (soluble fraction) tubulin. The pellet was resuspended in a volume of lysis buffer equal to the supernatant, and both were added an equal volume of gel sample buffer. Equal aliquots of polymerized and soluble fractions were loaded on SDS-PAGE, and western blots were probed with antibodies for tubulin. An advantage of this assay is that the amount of total protein loaded for each sample is irrelevant because the polymerized and soluble fractions are equalized for each pair, and it is the proportion of the polymerized to the soluble tubulin fraction that is measured [15].

2.7. Immunofluorescence assay

For fluorescence staining, HUVECs were plated on glass culture slides to nonconfluence and confluence in M199 medium containing 20% FCS, 0.5 h after the treatment of MDS-11 and CA4 (0.1% DMSO as negative control). Fixed preparations were obtained by exposing cells on culture slides to 4% paraformaldehyde in PBS for 10 min at 25 °C, followed by washing three times with PBS. Cells were blocked with 5% bovine serum albumin for 0.5 h, then incubated with tubulin antibody (Invitrogen, Carlsbad, CA) in 3% BSA (1:200) for 0.5 h, and followed by co-incubation with Cy3-conjugated secondary antibody (Invitrogen, Carlsbad, CA) diluted in 3% BSA (1:500) and phalloidin-FITC (Invitrogen, Carlsbad, CA) for 0.5 h. Coverslips were mounted on the slides with anti-fade agent and examined under Zeiss Confocal (Germany) Laser scanning microscope (40×, oil).

2.8. Viability assay in vitro [8]

HUVECs were assessed by initiating cultures in 96-well plates at 4.0×10^3 cells/well, followed by a 0.5 h exposure to the drug in medium. The plates were washed twice with PBS and incubated at 37 °C, and 5% CO_2 until the untreated control wells had become confluent. The surviving fraction was then assessed using MTT method. Each assay was performed at least three times, and a matrix of eight replicate wells per drug concentration was used. To assess the effect against quiescent HUVECs, the cells were first grown in 25 cm^2 flasks at 37 °C, 5% CO_2 and once confluent, exposed to the drug for 0.5 h, washed twice in PBS, trypsinized, and plated onto 96-well plates at 4×10^3 cells/well until untreated control wells had become confluent, and assayed using MTT method. Results were plotted following statistical analysis using the mean of at least seven replicates and ±SD.

2.9. Tube formation assay

HUVEC tube-structure formation on Matrigel was also conducted as described previously [16]. Briefly, 70 μl Matrigel (Becton Dickenson, Bedford, MA) at 4 °C was added to 96-well plates and then allowed to polymerize at 37 °C, 5% CO_2 for 1 h. HUVEC cells were suspended at the concentration of 2×10^4/0.1 ml in RPMI 1640 with 1% FCS. Cells were carefully layered on top of the polymerized gel and incubated for 8 h at 37 °C, 5% CO_2. 1 μM MDS-11P was added into each wells after tube formation have come into being for 0.5 h, 1 h except that negative controls were plated in RPMI 1640 with 1% FCS alone, then photographed under a microscope (CK40-F200, Olympus, Tokyo, Japan). Also 1 μM MDS-11 was added into each well after tube formation .The degree of tube disruption was assessed by counting the number of closed tubes in four random fields from each well.

2.10. Aortic ring assay

Vasculature disruption was also determined by the use of modified aortic ring assay technique. Briefly, rat aortic ring explant cultures were prepared by modification of protocols previously described [16]. 24-well plates were covered by 150 μl of Matrigel (Becton Dickenson, Bedford, MA). Aortic rings were prepared from male Sprague Dawley rats. Aortas were sectioned into 1 mm-long cross sections, rinsed several times with endothelial growth medium M199, placed on Matrigel in wells and covered with an additional 50 μl of Matrigel. The rings were cultured in 1 ml endothelial medium for several days. Cultures were incubated at 37 °C, in humidified CO_2 and the medium was replaced daily. After microvessels have developed to branch, wells were treated with MDS-11P except for negative control (0.1% DMSO) and taken a photograph at 0 h, 3 h and 9 h, respectively.

2.11. Animal administration and anticancer testing

For all experiments, mice were randomly allocated to various experimental groups. A549 (1×10^7 cells/mouse) and H22 (2×10^5 cells/mouse) were injected subcutaneously into the right flank of the nude mice and KM mice respectively. Animals were selected for drug single dose of treatment or multiple doses of treatment when their tumors reached about 100 mm^3. To guide *in vivo* studies, experiments were carried out to determine the most tolerated dose (MTD) of MDS-11P after i.p. administration. Because of ethical considerations, the MTD was not accurately determined but was approximated at 1500 mg/kg, a dose that resulted in no deaths in three male KM mice. Tumor growth of nude mice was determined by measuring the length (L) and width (W) of the tumor every other day with a caliper, and tumor volume was calculated on the basis of the following formula: the tumor volume (V) was calculated as follows: $V = (\text{length} \times \text{width}^2)/2$. The individual relative tumor volume (RTV) was calculated as follows: $RTV = V_t/V_0$, where V_t is the volume on each day, and V_0 is the volume at the beginning of the treatment. The therapeutic effect of the compounds was determined by the volume ratio of treatment to control (T/C). T/C (%) = 100% × (mean RTV of the treated group/mean RTV of the control group).

The mice bearing H22 were killed by dislocation of cervical vertebra 3 weeks after treatment. The tumor weights were measured and the inhibitory rates were calculated according to the following equation: rate of inhibition (%) = (mean tumor weight of control group − mean tumor weight of treated group)/mean tumor weight of control group × 100.

2.12. HE staining

Histological assessment was made to assess the induction of necrosis. A549 bearing mice were treated i.p. with single dose of MDS-11P or CA4P, and tumors were excised 4 h, 24 h later. After fixation in formalin, sections were made from paraffin embedded tumors and stained with H&E, and then the sections were imaged under a morphometric microscope. The necrotic fraction was then determined for these sections using the NIH imaging software Image J. For each tumor, the mean necrotic fraction was determined based on a minimum of three sections per tumor.

2.13. Immunohistochemical staining for CD31 and PCNA

Tumor tissues were fixed in a 10% buffered formalin solution and embedded in paraffin. The tissue sections (6 μm thick) were immunohistochemical stained with Santa Cruz ABC kit (Columbus, OH). Briefly, acetone fixed slides were blocked with horse normal serum for 0.5 h for nonspecific binding, and then incubated with a rat monoclonal antibody against mouse CD31 (Pharmingen BD, San Jose, CA) or a rabbit monoclonal antibody against mouse PCNA (Sigma, St. Louis, MO) for 2 h. Slides were washed with PBS and incubated with the second antibody for 0.5 h. After incubation with

streptavidin conjugated horseradish peroxidase (Sigma, St. Louis, MO) for 0.5 h, the slides were developed with 3, 3-diaminobenzidine or 3-amino-9-ethylcarbazole according to the manufacturer's instructions. Sections were counterstained with Gill's hematoxylin (Sigma, St. Louis, MO), and examined by light microscopy. For comparison, the slides were reviewed in all areas but the photographs were taken from the same area: the midpoint between the peripheral membrane and the center of the tumor (the cutting edge of the half tumor). Representative photos were presented in the results.

2.14. Perfused vascular volume assay

Functional vascular volume was assessed in control tumors and at selected times after drug treatment using Hoechst 33342 (Sigma, St. Louis, MO), as reported previously [17]. The fluorescent DNA-binding dye was dissolved in pure water at 1 mg/ml and injected i.v. at a dose of 10 mg/kg. Tumors were excised and frozen 1 min later. Sections were cut at 3 levels and observed under UV illumination. Perfused vessels were identified by their fluorescent outlines and vascular volumes were determined using a random point scoring system based on that described by Chalkley. At least 100 fields were scored at each of the 3 tumor levels and the results for treated tumors were expressed as a percentage of control values.

2.15. Pharmacokinetics study

Male KM mice were i.p. with 100 mg/kg MDS-11P at various times before sacrifice and exsanguinations with five animals used at each time point. Blood samples were collected into heparin and centrifuged at 3000 × *g* for 5 min; separated plasma was stored at −20 °C. Aliquots (300 μl) were treated with methanol (900 μl) and an internal standard, centrifuged (10,000 × *g*) for 10 min, and the supernatants dried in a centrifugal evaporator. Samples were reconstituted in 45% aqueous methanol analyzed for both MDS-11P and MDS-11 by high-performance liquid chromatography on a 4.6 mm × 250 mm Venμsil RPB column (Agela technologies, Tianjin, China) with a gradient system [mobile phase *A* = 55% 50 mM potassium dihydrogen phosphate (pH 2.2), 45% methanol; mobile phase B = acetonitrile]. The gradient was run initially at 0% B (0–11 min) but increased to 45% over 4 min and was maintained for an additional 14 min, then returning to the start conditions from 28 to 30 min. Detection was by the Gilson 152 UV/VIS Detectors (Gilson Medical Electronics, Middleton, WI) at 288 nm. Concentrations of MDS-11P and MDS-11 were calculated from respective calibration curves. Pharmacokinetic parameters were analyzed using computer software called 3p97.

2.16. Statistical analysis

Results were expressed as the mean ± standard deviation (SD). The data was analyzed by the Student's *t*-test; *P*-values of <0.05 were considered statistically significant ($^{*}P < 0.05$; $^{**}P < 0.01$, $^{***}P < 0.001$).

3. Results

3.1. MDS-11 binds to tubulin and inhibits tubulin polymerization

To quantitatively characterize the binding of MDS-11 to tubulin, the association and dissociation kinetics of their interaction were examined by SPR measurements. Typical sensorgrams of MDS-11–tubulin interaction were obtained at 200 μM, 400 μM, 800 μM and 1000 μM of MDS-11 when biotinylated tubulin was immobilized onto a streptavidin-coated sensor chip (Fig. 2A). Similar binding parameters were obtained for CA4–tubulin interaction (Fig. 2B) and colchicine–tubulin interaction (Fig. 2C) by SPR under similar conditions. The dissociation constant (K_d values) of MDS-11 was

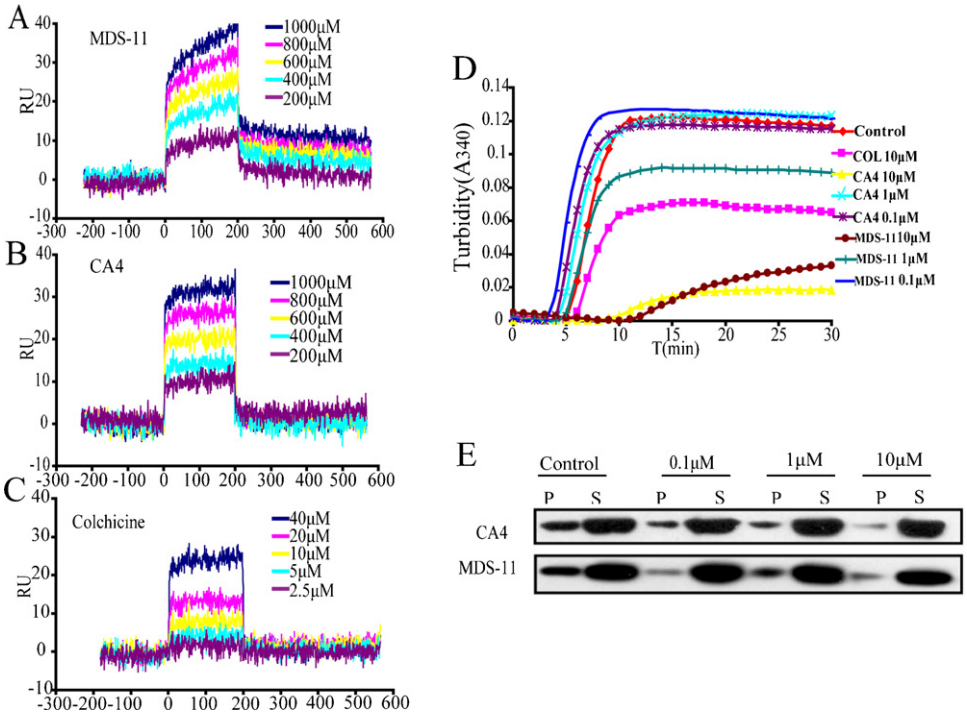

Fig. 2. Affinity analysis of tubulin bound to MDS-11 (A), CA4 (B) and colchicine (C) by SPR. Tubulin was immobilized on CM5 sensor chips, and different concentrations of MDS-11 or CA4 or colchicine were injected over the sensor chip surface. Changes in mass were recorded as resonance units (Ru). Dissociation constants were calculated using BIACORE software 3.1. (D) MDS-11 inhibited tubulin polymerization at molecular level. MDS-11 at various concentrations were mixed with tubulin from porcine brains, tubulin polymerization was initiated and monitored by turbidity changes at 340 nm using a spectrometer. (E) MDS-11 inhibited tubulin polymerization at cellular level. HUVECs were harvested in lysis buffer and centrifuged to separate polymerized fraction from soluble fraction, then both fractions were analyzed by western blot.

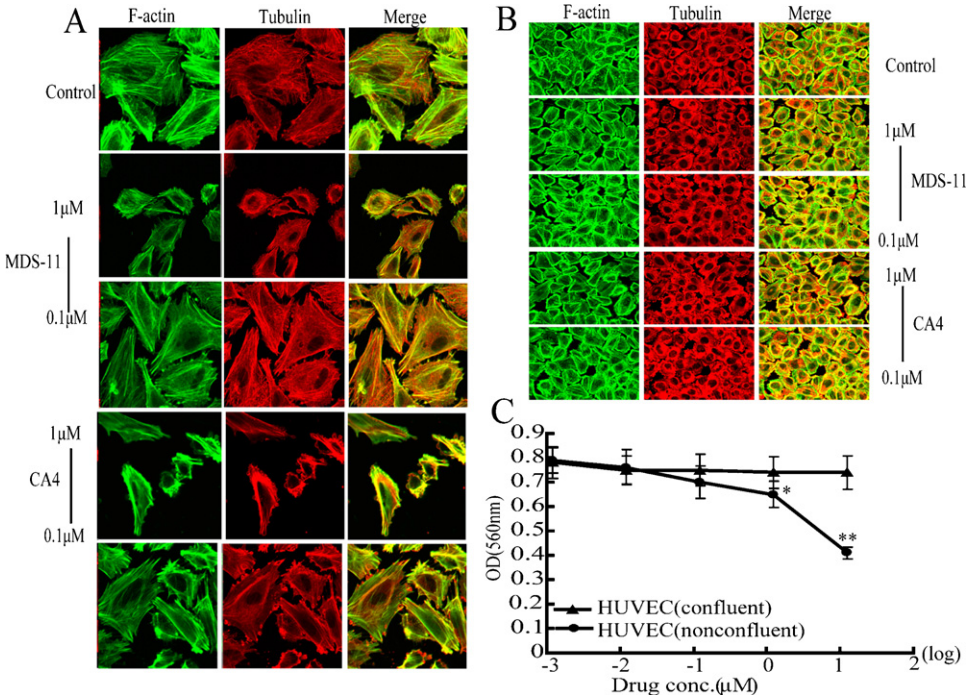

Fig. 3. Effects of MDS-11 on microtubules and actin microfilament in nonconfluent HUVECs (A) and confluent HUVECs (B). HUVECs with nonconfluence and confluence were treated for 0.5 h by MDS-11 and CA4, then fixed and incubated with tubulin antibody followed by Cy3-conjugated secondary antibody and phalloidin-FITC for 0.5 h, then observed and photographed under confocal. (C) Effects of MDS-11 on viability of confluent and nonconfluent HUVECs. HUVECs with nonconfluence and confluence exposed to MDS-11 in medium for 0.5 h, then washed the test drug and cultured until cells in the untreated control wells had become confluent, and determined by MTT method. Statistical significance ($P < 0.05$) relative to the confluent HUVECs is designated by an asterisk.

1.77×10^{-3} M, which was comparable with that of CA4 (2.55×10^{-3} M), but large than that of colchicine (5.53×10^{-4} M). These values are consistent with the concentrations at which MDS-11 elicits its biological activities, considering that tubulin is polymeric macromolecules and strong binding activity may inhibit reversible dissociation. These data indicate that MDS-11 is a potent tubulin binding agent.

The kinetics of tubulin polymerization was further monitored *in vitro* using purified tubulin. As shown in Fig. 2D, MDS-11, CA4 and colchicine at a dose of 10 μM dramatically inhibited the tubulin polymerization. MDS-11 suppressed the polymerization of the purified tubulin even at 1 μM, while CA4 at the same concentration failed to exhibit obvious inhibitory effect, These data suggested that MDS-11 had higher inhibitory activity toward tubulin polymerization than CA4 whereas. Colchicine presented the lowest activity on tubulin polymerization among the three compounds.

Cellular microtubules are always in the process of polymerization and depolymerization. Tubulin inhibitors could change their dynamics by promoting or inhibiting polymerization. To examine whether MDS-11 affects tubulin polymerization in cells, we exposed HUVECs to MDS-11 and CA4 for 0.5 h and then separated the intracellular polymerized and soluble tubulin by ultracentrifugation. Both the pellet (containing the polymerized tubulin) and the supernatant (containing the soluble tubulin) were subjected to immunoblotting. The result showed that MDS-11 decreased the cellular polymerized tubulin fractions in a concentration-dependent manner in the range of 0.1 μM to 10 μM (Fig. 2E), which was similar to CA4.

3.2. The selective effects of MDS-11 on confluent and nonconfluent HUVEC cells

Differences in the physiology of immature tumor versus mature normal vasculature provide an opportunity for the selective disruption of tumor blood flow. It has been reported that confluent endothelial cells in monolayers can mimic the scenario of mature and quiescent endothelial cells whereas nonconfluent and proliferating cells as immature ones [18]. A study was made of the morphological effects of MDS-11 on confluent and nonconfluent HUVEC monolayer cultures to model the endothelial cells of mature and immature vasculature, respectively. As shown in Fig. 3A, MDS-11 caused the disruption of microtubules within 0.5 h at as low as 0.1 μM as shown by the disappeared cross-filaments in cells. At higher concentrations, MDS-11 treated cells finally shrivelled as a result of enormous damage to microtubules. The remarkable increase of stress fibers were also observed at the same time, which is the feature of vascular disruption agent. However, only slight effects were found on the confluent HUVEC cells at up to 1 μM (Fig. 3B). We also found that confluent HUVEC monolayers exhibited the dense peripheral band of actin and tubulin, whereas the actin and tubulin microfilament distribution of the nonconfluent cells appeared diffused, which was in agreement with the previous studies [19]. In these experiments, we could barely detect the difference between MDS-11 and CA4. All together, these results indicated that differences in cytoskeletal organization may contribute to differential sensitivity to MDS-11, and suggested that MDS-11 might have selective effects on tumor vascular. To further quantitatively investigate the roles of distinct sensitivity to MDS-11 in HUVEC cells at different growth state, confluent and nonconfluent HUVEC cells were exposed to MDS-11 for 0.5 h, then MTT assay was utilized until cells in untreated control wells had become confluent. Fig. 3C showed that MDS-11′ selective toxicity was primarily directed toward nonconfluent endothelial cells in dose dependent manner.

3.3. Vasculature disrupting effects of MDS-11 and its prodrug on HUVEC-formed vascular tube

To investigate the effects of MDS-11 on vasculature disruption, we first determined the effects of MDS-11 on HUVEC-formed

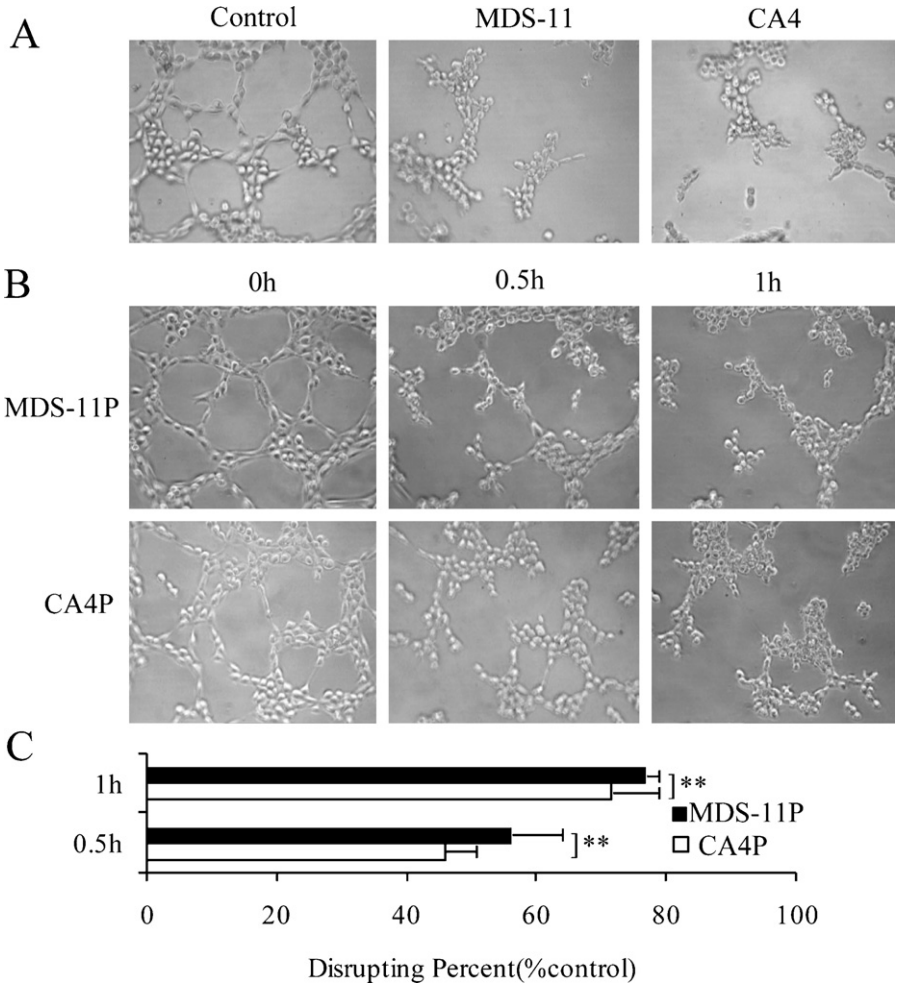

Fig. 4. MDS-11 and MDS-11P disrupted the HUVEC-formed vascular tube. HUVEC cells were carefully layered on top of the polymerized matrigel and incubated for 8 h for formation of HUVEC tube, MDS-11 and MDS-11P were added respectively after tube formation. (A) MDS-11 at 0.1 μM was added into each wells, then photographed under a microscope after 0.5 h treatment. (B) MDS-11P and CA4P at 0.1 μM was added into each wells, then photographed under a microscope at various times treatment. (C) Statistical chart of (B). $^{**}P < 0.01$ versus CA4P ($n = 3$).

vascular tube. Distinct from the study of angiogenesis inhibitor, MDS-11 was added after tube formation and results were observed at early time points. In the control group, HUVECs formed a mesh of tubes on a matrigel substratum after 8 h. The tubes' structures were severely damaged when cells were exposed to MDS-11 in dose dependent manner, the disrupting rate was nearly 90% after 1 h treatment (Fig. 4A). MDS-11P, the prodrug of MDS-11, had similar effects. Notably, it seemed that MDS-11P was more effective than CA4P at early stage. We speculate that the difference was due to the faster cleavage of phosphate group of MDS-11P by endogenous nonspecific phosphatases than that of CA4P (Fig. 4B and C).

3.4. Vasculature disrupting effects of MDS-11 on microvessels from aortic rings

Next, we examined the effects of the compound on the integrity of microvessel from aortic rings. The microvessels that grow out from aortic rings recruit smooth muscle cells and pericytes to associate with the endothelial cell tube, meaning that they are anatomically similar to normal neovessels *in vivo* [20]. Similarly MDS-11 was added after microvessels formed. As shown in Fig. 5 compared with the effects on HUVEC-formed vascular tube, MDS-11 did not disrupt microvessel integrity until 3 h,when visible broken small particles were observed. In addition, it was noticed that CA4 exhibited more potent effect than MDS-11 at this experimental model as more particles were seen during treatment of 1 μM CA4. These results suggest that MDS-11 appears to selectively disrupt the vasculature in tumor tissue *in vivo* and is less toxic to vasculature in normal tissue than CA4.

3.5. Early effects of MDS-11P on disrupting tumor vasculature in vivo

A549 human lung carcinoma cell line xenograft was used in this experiment. CD31 is the most specific and sensitive endothelial marker currently available. It is present on most capillaries and is a reliable epitope for immunostaining. Fig. 6A and B showed the typical reduction of tumor blood vasculature number after MDS-11P treatment at a single dosage of 100 mg/kg determined by immunohistochemical staining with the antibody reactive to CD31 in brown color. Compared with control, tumor blood vasculature numbers were reduced as early as 4 h after drug administration, 24 h later, CD31 could barely be detected. The PCNA positive can be used as an index of cell proliferation. Fig. 6C showed that cell proliferation in the whole tumor decreased after 4 h MDS-11P treatment, and then continued to reduce until 24 h, which was in accordance with the results of HE staining. The HE staining suggested that 24 h after a single i.p. injection of 100 mg/kg MDS-11P, there was a massive area of necrosis within tumor, and the viable rim was also been observed, which suggested that MDS-11P

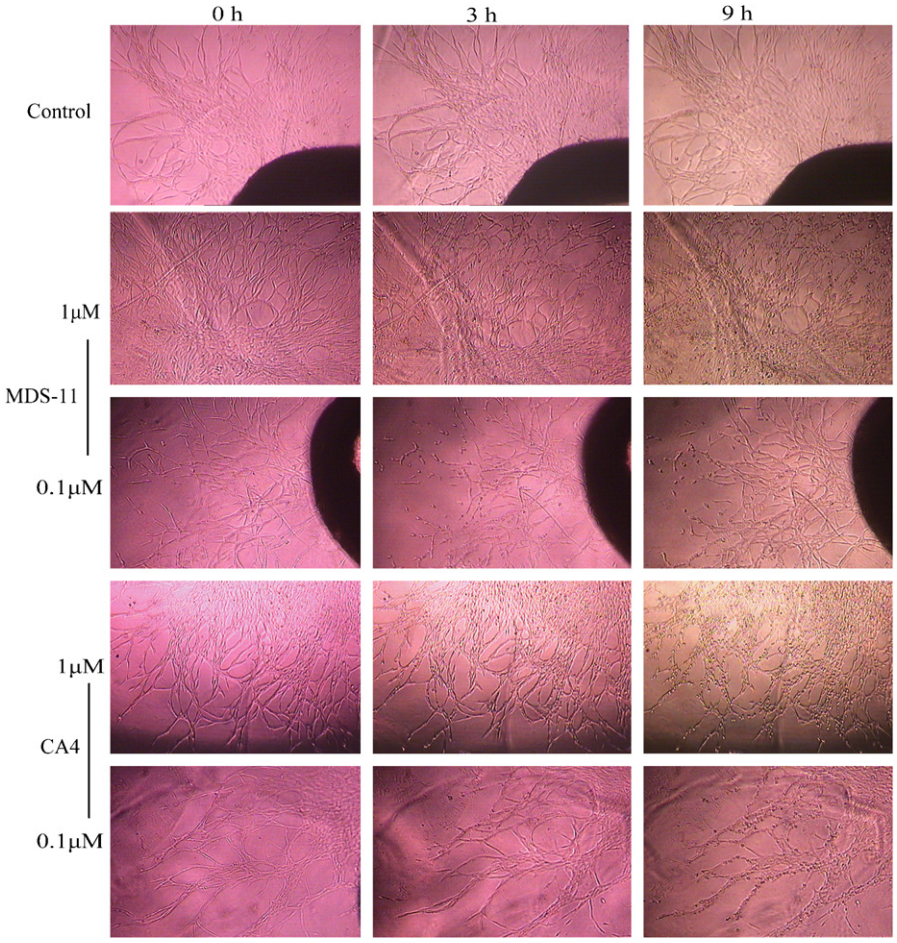

Fig. 5. Aortic ring assay observed the disrupting effect of MDS-11. After microvessels have developed to branch, MDS-11 at 1 μM and 0.1 μM respectively was added into each wells, then photographed under a microscope at various times. MDS-11 did not rapidly disrupt microvessel integrity until 3 h.

was more effective in the tumor center than in the tumor periphery like other VDAs (Fig. 6D). These results demonstrated that MDS-11P could selectively destroy vasculature of tumor tissue and induce extensive secondary tumor cell death. Likewise, no obviously different effects were found compared with CA4P at single dose treatment.

Furthermore, the effects on vascular shutdown of MDS-11P were further consolidated by counting the number of perfused tumor blood vessels labeled with nucleus dye Hoechst 33342 under fluorescence microscope. These results showed that within 24 h of treatment with either CA4P or MDS-11P, a significant reduction in perfused vessels was apparent by 69.74%. However, after 48 h and 72 h of drug exposure, some vascular recovery occurred from the viable rim of tumor tissue in a time-dependent manner, which was also observed in CA4P-treated mice (Fig. 6E and F).

3.6. Pharmacokinetics study

The plasma concentration versus time of MDS-11 and MDS-11P was evaluated in KM mice after a single i.p. dose of 100 mg/kg MDS-11P (Fig. 7). Median and overall statistical summaries of pharmacokinetic parameters with two-compartment models are outlined in Table 1. Rapid MDS-11P activation followed by rapid elimination of MDS-11 was apparently observed. The maximum plasma concentrations of MDS-11P or MDS-11 were achieved in less than 5 min interval ($T_{max} < 10$ min), and the high level of the MDS-11 phosphate prodrug was detected in plasma (C_{max} = 40 mg/l,) with a high conversion to the active drug MDS-11 (C_{max} = 36.3 mg/l), indicating a rapid conversion of the prodrug MDS-11P to MDS-11. A possible explanation for this observation is that, the phosphate moieties attached to the MDS-11 hydroxyl group may be accessible for the alkaline phosphatase. The mean terminal half-life of MDS-11 was 26.7 min, as estimated from at least five time points, indicating that MDS-11 can be rapidly cleared away *in vivo*.

3.7. The antitumor effects of MDS-11P in vivo

To elucidate the antitumor effects of MDS-11P *in vivo*, the tumor growth in H22 hepatocarcinoma bearing mice following MDS-11P multiple doses of treatments was investigated. In this experiment, MDS-11P was administrated i.p. twice a day for 3 weeks after tumor size reached to 100 mm^3 in volume. The mice were weighed twice per week and the tumor weights were measured after the mice bearing H22 were killed by dislocation of cervical vertebra. As shown in Fig. 8A and B, MDS-11P significantly inhibited the growth of H22 subcutaneous tumor ($P < 0.01$) in a dose-dependent manner, with 25.4%, 59.4% and 70.4% reduction, at the doses of 25 mg/kg, 50 mg/kg and 100 mg/kg respectively. The inhibitory rate of MDS-11P was lower than that of CA4P ($P < 0.05$) when mice were treated at same dosage of 50 mg/kg. However, the weight loss was also much higher in CA4P treated mice ($P < 0.01$), as MDS-11P did not significantly decrease the body weight ($P > 0.05$) at this dosage. Moreover, even at the higher doses of 100 mg/kg, where MDS-11P had similar inhibitory rate to 50 mg/kg of CA4P, MDS-11P caused less weight loss ($P < 0.05$).

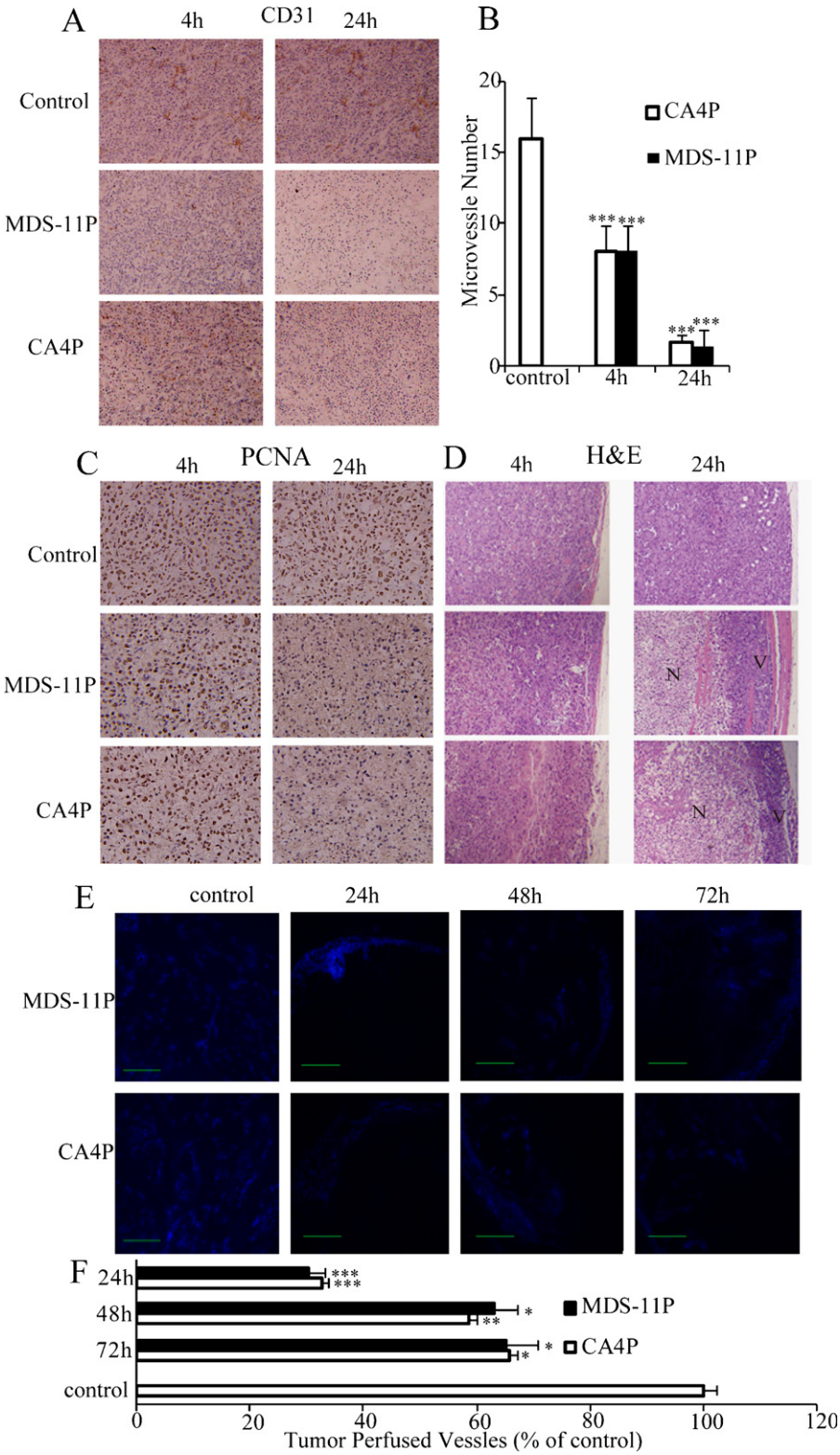

Fig. 6. MDS-11P at single dose disrupted tumor vasculature and induced tumor necrosis *in vivo* by immunohistochemistry staining. Tumor tissues were fixed in a 10% buffered formalin solution and embedded in paraffin. The tissue sections (6 μm thick) were immunohistochemical stained. (A) CD31 immunohistochemistry staining of tumor after 100 mg/kg MDS-11P treatment. ×200 magnification. (B) Statistical chart of (A). $^{***}P < 0.001$ versus control. (C) PCNA immunohistochemistry staining of tumor after 100 mg/kg MDS-11 treatment. ×200 magnification. (D) HE staining of tumor after 100 mg/kg MDS-11P treatment. (N: necrosis, V: viable rim). ×200 magnification. (E) A reduction in perfused vasculature (blue staining) of H22 tumors. After treatment with a single i.p. injection of 100 mg/kg MDS-11P for 24, 48, 72 h, the fluorescent DNA-binding dye Hoechst 33342 was injected i.v. at a dose of 10 mg/kg, then tumors were excised and frozen 1 min later, and sections (6 μm thick) were observed and photographed under UV illumination. Scale bar: 500 μm. (F) Statistical chart of (E). $^{*}P < 0.05$, $^{**}P < 0.01$, $^{***}P < 0.001$ versus control. (For interpretation of the references to color in this figure legend, the reader is referred to the web version of the article.)

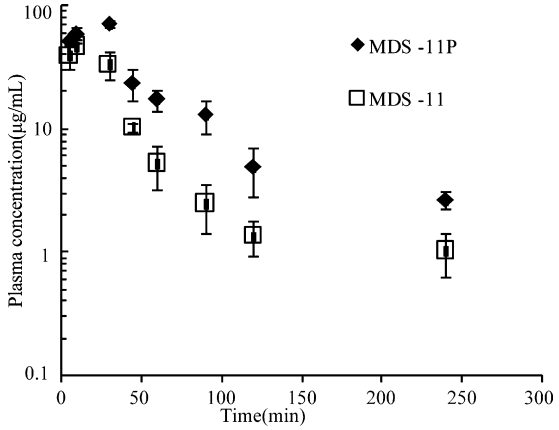

Fig. 7. Plasma levels of MDS-11P (◆) and MDS-11 (□) in KM mice after a single i.p. dose of MDS-11P (100 mg/kg). Each point, the mean of at least 5 mice. Error bars, ±SD.

Fig. 8D represents the tumor growth inhibition of A549-bearing nude mice after multiple doses of treatments of MDS-11P in comparison with the control group. Relative tumor volumes in mice treated with MDS-11P at 50 mg/kg twice a day were inhibited by 60.5%. The changes in body weights between the control and the MDS-11P-treated mice ($n = 5$) were not remarkably different.

4. Discussion

Differences in the physiology of immature tumor versus mature normal vasculature provide an opportunity for the selective disruption of tumor blood flow, leading to tumor death. And an alternative to this antiangiogenic approach is to target the existing tumor vasculature [21,1,2], a number of agents that target tumor blood vessels have now been identified and the lead candidate CA4P has entered clinical trials [22], which encourages people to develop more efficient VDAs. In the present paper, we firstly demonstrated that MDS-11 and its prodrug MDS-11P, are potential VDAs. Several years ago, MDS-11 has only been recognized as a cytotoxic compound with treatments of 72 h on a variety of tumor cell lines [11].

Table 1
Pharmacokinetic data summary for MDS-11P and MDS-11 in plasma after i.p. administration of the prodrug MDS-11P at 100 mg/kg.

	T_{max} (min)	C_{max} (mg/l)	$T_{1/2}$ (min)	CL ($L\,kg^{-1}\,min^{-1}$)	$AUC_{0-4\,h}$ ($mg\,min\,L^{-1}$)
MDS-11P	6.98	39.1	40.0	0.051	1959.0
MDS-11	10.0	36.3	26.7	0.067	1476.7

Historically, there have been reports of a number of tubulin-binding agents that destabilize the tubulin cytoskeleton leading to a disruption of the tumor vasculature. These agents include colchicine, vincristine, and vinblastine, which have been found to be antitumorigenic but only at doses close to their MTD, and direct tumor cell cytotoxicity is the predominant mechanism of the action [23]. Developments of second-generation tubulin depolymerizing agents, which disrupt the tumor vasculature at doses well below their MTD have allowed this mechanism to be reinvestigated [24]. CA4 is a tubulin-binding agent and significantly reduces vascular function, even at doses down to one-tenth of the MTD. In this present study, surface plasmon resonance assay was utilized to screen the compound bound to tubulin, in which biotinylated tubulin was immobilized onto a streptavidin-coated CM5 sensor

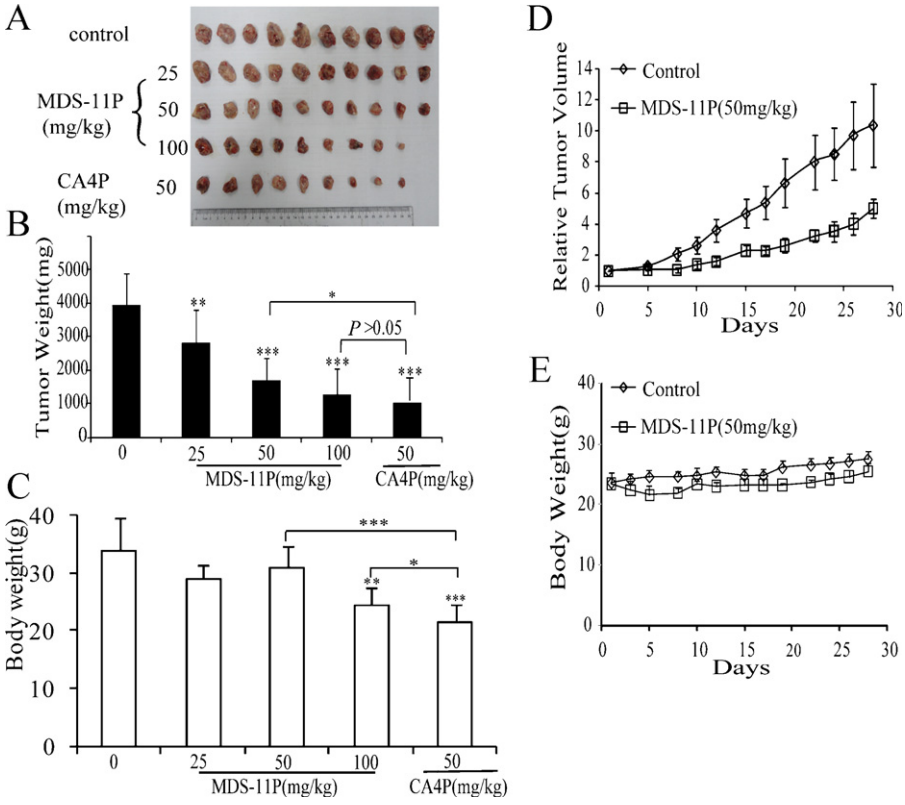

Fig. 8. The antitumor effects of MDS-11P *in vivo* following MDS-11P multiple doses of treatments. (A) Anti-tumor effects of MDS-11P on H22-bearing mice. Quantification results were expressed as tumor weight (B) or body weight (C). Each point, the mean of 9–10 tumors or mice. Error bars, ±SD. (D) Anti-tumor effect of MDS-11P on A549-bearing mice. (E) Change in body weight of mice bearing tumor induced by MDS-11P. Each point, the mean of at least 5–6 tumors or mice. Error bars, ±SD.

chip with the tubulin binding site exposed. Our efforts yielded the compound MDS-11, which bound to tubulin with its K_d comparable to that of CA4 from over 30 compounds rationally designed and synthesized. In addition, in our studies, we found that MDS-11 inhibited the polymerization of tubulin in a cell-free system, was even superior to CA4, and western blot assay further confirmed depolymerization of microtubules in HUVEC cells induced by MDS-11. Collectively, these results suggest that MDS-11 is a tubulin-binding agent with bioactivity.

The depolymerization of the tubulin network in tumor vascular endothelial cells is responsible for the endothelial cell shape change and subsequent vascular disruption observed in tumors treated with VDAs such as CA4P and ZD6126 [25]. Differences between tumor and normal tissue endothelial cells may influence the primary damage inflicted on them such as differences in proliferation rate [8], post-translational modifications of tubulin [26,27]. It is also believed that tumor in mature endothelial cells rely on a cytoskeleton primarily of tubulin to maintain their shape, whereas mature endothelial cells rely on both tubulin and actin [28,29], thereby enhancing tumor endothelial cells as the primary target [29,30]. Confluent endothelial cells in monolayers can be models as mature, quiescent endothelial cells whereas nonconfluent, proliferating cells as immature ones [8]. New generation tubulin-binding agents should induce cell shape changes in proliferating cells but not quiescent endothelium to depress the side effects to normal tissue vasculature [8]. In this paper, changes in the cellular microtubule network were observed more obviously in nonconfluent HUVECs than in confluent after exposed to MDS-11. In addition, we found that MDS-11 selectively reduced the activity of nonconfluent endothelial cells but not confluent ones after 30 min treatment. Take together, these results suggest that MDS-11would be a potential tumor vascular targeting agent with high selectivity.

Many tumors bear the hallmarks of immaturity for lack of support by vascular mural cells such as pericytes and smooth muscle cells [31]. HUVEC-formed vascular tube and microvessel from aortic rings are two models simulating different status of neovessels *in vivo*. Microvessels from aortic rings are closer to mature vessels because of possessing pericytes and smooth muscle cells, while HUVEC-formed vascular tube is similar to vasculature in tumor. In our experiment, unlike angiogenesis assay, the compound was treated after formation of tube and vessel. We found that MDS-11 and CA4 had equivalent activities in damaging vascular tubes. However, microvessels from aortic rings had a greater tolerance to both compounds compared with HUVEC-formed vascular tubes, CA4 was noticed to exhibit more potent effects on the microvessel from aortic rings than MDS-11P even at 0.1 μM. The ability of MDS-11 to induce dramatic damage preferentially in HUVEC-formed vascular tube suggests that immature tumor vasculature may be selectively targeted, and the MDS-11 appears to be VDAs with less side effects than CA4.

Hallmark characteristics of VDAs are reduction in microvessel density, induction of widespread tumor necrosis, secondary tumor cell death due to ischemia, and the presence of a surviving rim of neoplastic cells at the tumor periphery [1,32]. The *in vivo* immunohistochemical analysis with lung tumor models confirmed the selective effects of MDS-11P on tumor vasculature when administered single dose to tumor-bearing mice. At 100 mg/kg, rapid and prolonged vasculature damage was evident, and human tumor models showed extensive necrosis after 24 h accompanied by inhibition of tumor cells proliferation. Tumor cells distant from the blood vessels died at earlier time points than those adjacent to the blood vessel. This pattern of cell death is consistent with the death because of nutrient starvation rather than direct cytotoxicity, which provides further support for vascular damage-mediated mechanism of MDS-11P. MDS-11P was observed to have prominent antitumor activities *in vivo* at doses around one-fifteenth of the MTD (1500 mg/kg), which features a broad therapeutic window compared to many known combretastatin derivatives showing activity at doses around one-third [26] to one-tenth [27] of the MTD.

Although MVD has been reported to be a useful prognostic indicator in a number of tumor types, its value as an indicator of the efficacy of vascular-targeting therapies is limited [33]. Therefore, further investigations using Hoechst 33342 to examine perfused vascular volume revealed a significant reduction in perfused tumor vasculature following treatment of mice with MDS-11P. However, the increase of fluorescence after 48 h initial treatment like CA4 suggests that some neovascularization may account for, at least partially, the recovery in tumor growth observed before. These observations are consistent with a viable rim of proliferating tumor cells detected by HE staining. These results suggest that the MDS-11P also has the characteristics of other VDAs and combination treatment is required for MDS-11P.

The antitumor efficacy was demonstrated in two kinds of tumor xenograft-bearing mice with multiple doses of MDS-11P, and high tumor growth inhibition rate was acquired. Although, MDS-11P has lower antitumor effect than CA4P at 50 mg/kg twice a day, we noticed that the weight loss of mice treated by MDS-11P was much less than that of CA4P, which is tenable even MDS-11P at 100 mg/kg with similar antitumor activity to CA4P at 50 mg/kg since the pharmacokinetic study of MDS-11P in mice indicated a much faster elimination of the active drug, comparing with 35 min of half time for CA4 as reported [29], and the fact that MDS-11P with rapid reversibility to MDS-11 is more effective than CA4P in disrupting HUVEC-formed vascular tube, at early stage, and also MDS-11 selective toxicity was primarily directed toward nonconfluent and immature endothelial cells within 0.5 h, it is possible that a short exposure *in vivo* to MDS-11P is adequate to cause rapid damage to tumor vasculature, therefore avoiding toxicities due to a prolonged disruption of microtubules in other normal tissues.

Overall, the studies reported here show that well-tolerated MDS-11P promises as a novel vascular-targeting agent with similar efficient and low toxicity compared with CA4P, taking the stability of MDS-11P into consideration, we believe that MDS-11P is worthy of further development for antitumor drug.

Acknowledgements

This work was supported by the grants from National High-tech R&D Program (2007AA09Z405) of China and Program for Changjiang Scholars and Innovative Research Team in University (IRT0944).

References

[1] Tozer GM, Kanthou C, Baguley BC. Disrupting tumour blood vessels. Nat Rev Cancer 2005;5:423–35.
[2] Thorpe PE. Vascular targeting agents as cancer therapeutics. Clin Cancer Res 2004;10:415–27.
[3] Siemann DW. The unique characteristics of tumor vasculature and preclinical evidence for its selective disruption by tumor-vascular disrupting agents. Cancer Treat Rev 2011;37:63–74.
[4] Heath VL, Bicknell R. Anticancer strategies involving the vasculature. Nat Rev Clin Oncol 2009;6:395–404.
[5] McGown AT, Fox BW. Structural and biochemical comparison of the anti-mitotic agents colchicine, combretastatin A4 and amphethinile. Anticancer Drug Des 1989;3:249–54.
[6] Pettit GR, Temple CJ, Narayanan VL, Varma R, Simpson MJ, Boyd MR, et al. Antineoplastic agents 322. Synthesis of combretastatin A-4 prodrugs. Anticancer Drug Des 1995;10:299–309.
[7] Stevenson JP, Rosen M, Sun W, Gallagher M, Haller DG, Vaughn D, et al. Phase I trial of the antivascular agent combretastatin A4 phosphate on a 5-day schedule to patients with cancer: magnetic resonance imaging evidence for altered tumor blood flow. J Clin Oncol 2003;21:4428–38.

[8] Dark GG, Hill SA, Prise VE, Tozer GM, Pettit GR, Chaplin DJ. Combretastatin A-4, an agent that displays potent and selective toxicity toward tumor vasculature. Cancer Res 1997;57:1829–34.
[9] Grosios K, Holwell SE, McGown AT, Pettit GR, Bibby MC. In vivo and in vitro evaluation of combretastatin A-4 and its sodium phosphate prodrug. Br J Cancer 1999;81:1318–27.
[10] Pettit GR, Toki BE, Herald DL, Boyd MR, Hamel E, Pettit RK, et al. Antineoplastic agents, 410. Asymmetric hydroxylation of trans-combretastatin A-4. J Med Chem 1999;42:1459–65.
[11] Wang L, Woods KW, Li Q, Barr KJ, McCroskey RW, Hannick SM, et al. Potent, orally active heterocycle-based combretastatin A-4 analogues: synthesis, structure-activity relationship, pharmacokinetics, and in vivo antitumor activity evaluation. J Med Chem 2002;45:1697–711.
[12] Baudin B, Bruneel A, Bosselut N, Vaubourdolle M. A protocol for isolation and culture of human umbilical vein endothelial cells. Nature Protocols 2007;2:481–5.
[13] Tirian L, Hlavanda E, Olah J, Horvath I, Orosz F, Szabo B, et al. TPPP/p25 promotes tubulin assemblies and blocks mitotic spindle formation. Proc Natl Acad Sci USA 2003;100:13976–81.
[14] Shelanski ML, Gaskin F, Cantor CR. Microtubule assembly in the absence of added nucleotides. Proc Natl Acad Sci USA 1973;70:765–8.
[15] Kanthou C, Tozer GM. The tumor vascular targeting agent combretastatin A-4-phosphate induces reorganization of the actin cytoskeleton and early membrane blebbing in human endothelial cells. Blood 2002;99:2060–9.
[16] Staton CA, Stribbling SM, Tazzyman S, Hughes R, Brown NJ, Lewis CE. Current methods for assaying angiogenesis in vitro and in vivo. Int J Exp Pathol 2004;85:233–48.
[17] Hill SA, Chaplin DJ, Lewis G, Tozer GM. Schedule dependence of combretastatin A4 phosphate in transplanted and spontaneous tumour models. Int J Cancer 2002;102:70–4.
[18] Lunt SJ, Akerman S, Hill SA, Fisher M, Wright VJ, Reyes-Aldasoro CC, et al. Vascular effects dominate solid tumor response to treatment with combretastatin A-4-phosphate. Int J Cancer 2010.
[19] Davis PD, Dougherty GJ, Blakey DC, Galbraith SM, Tozer GM, Holder AL, et al. ZD6126: a novel vascular-targeting agent that causes selective destruction of tumor vasculature. Cancer Res 2002;62:7247–53.
[20] Goodwin AM. In vitro assays of angiogenesis for assessment of angiogenic and anti-angiogenic agents. Microvasc Res 2007;74:172–83.
[21] Kanthou C, Tozer GM. Microtubule depolymerizing vascular disrupting agents: novel therapeutic agents for oncology and other pathologies. Int J Exp Pathol 2009;90:284–94.
[22] Rustin GJ, Shreeves G, Nathan PD, Gaya A, Ganesan TS, Wang D, et al. A Phase Ib trial of CA4P (combretastatin A-4 phosphate), carboplatin, and paclitaxel in patients with advanced cancer. Br J Cancer 2010;102:1355–60.
[23] Thorpe PE, Chaplin DJ, Blakey DC. The first international conference on vascular targeting: meeting overview. Cancer Res 2003;63:1144–7.
[24] Siemann DW, Chaplin DJ, Walicke PA. A review and update of the current status of the vasculature-disabling agent combretastatin-A4 phosphate (CA4P). Expert Opin Investig Drugs 2009;18:189–97.
[25] Marrelli M, Conforti F, Statti GA, Cachet X, Michel S, Tillequin F, et al. Biological potential and structure-activity relationships of most recently developed vascular disrupting agents: an overview of new derivatives of natural combretastatin a-4. Curr Med Chem 2011;18:3035–81.
[26] Galbraith SM, Chaplin DJ, Lee F, Stratford MR, Locke RJ, Vojnovic B, et al. Effects of combretastatin A4 phosphate on endothelial cell morphology in vitro and relationship to tumour vascular targeting activity in vivo. Anticancer Res 2001;21:93–102.
[27] Tozer GM, Kanthou C, Parkins CS, Hill SA. The biology of the combretastatins as tumour vascular targeting agents. Int J Exp Pathol 2002;83:21–38.
[28] Bayless KJ, Johnson GA. Role of the cytoskeleton in formation and maintenance of angiogenic sprouts. J Vasc Res 2011;48:369–85.
[29] Siemann DW, Mercer E, Lepler S, Rojiani AM. Vascular targeting agents enhance chemotherapeutic agent activities in solid tumor therapy. Int J Cancer 2002;99:1–6.
[30] Ghosh K, Thodeti CK, Dudley AC, Mammoto A, Klagsbrun M, Ingber DE. Tumor-derived endothelial cells exhibit aberrant Rho-mediated mechanosensing and abnormal angiogenesis in vitro. Proc Natl Acad Sci USA 2008;105:11305–10.
[31] Eberhard A, Kahlert S, Goede V, Hemmerlein B, Plate KH, Augustin HG. Heterogeneity of angiogenesis and blood vessel maturation in human tumors: implications for antiangiogenic tumor therapies. Cancer Res 2000;60:1388–93.
[32] Siemann DW, Chaplin DJ, Horsman MR. Vascular-targeting therapies for treatment of malignant disease. Cancer 2004;100:2491–9.
[33] Hlatky L, Hahnfeldt P, Folkman J. Clinical application of antiangiogenic therapy: microvessel density, what it does and doesn't tell us. J Natl Cancer Inst 2002;94:883–93.